TOCAD

Thermohaline circulation and Ocean Changes using ARGO Data

Un projet soutenu par le **Groupe Mission Mercator/Coriolis** (AO 2007).
Action ciblée **EuroArgo**

Responsable scientifique : Fabienne Gaillard

Laboratoire de physique des Océans (UMR 6523-IUEM)

Ifremer, Centre de Brest, BP 70, 29280 Plouzané

Tél : 33-2-98-22-42-88   Courriel : fabienne.gaillard@ifremer.fr

Rapport annuel 2008/ Annual report 2008

12/01/2009

Contributeurs/Contributors

C. Cabanes, B. Ferron, F. Gaillard, K. von Schuckmann,
LPO, UMR 6523 - IUEM
Centre Ifremer de Brest

1 Introduction

During the first year of the TOCAD project, 4 studies in relation with Argo have been carried.

The first study focused on developping automatic methods for the quality control of the Argo dataset. Diagnostics performed on the analysis residuals allow to identify salinity offsets and drifts, which are the most common problems related to the sensor behavior. It has been shown also how the temperature residuals could converted into a pressure residual to detect the problem of pressure laelling that occured on some Solo floats.

Using the same analysis technique (ISAS) the temperature and salinity fields were produced for the world ocean during the period 2003-2007. The mean field and annual cycle have been compared to the previous WOA05 climatology to estimate the decadal variability. The global warming is confirmed, the strongest signal being observed in the North Atlantic. Salinity changes follow a more complex pattern. The time series of the mean global steric height shows a trend to an increase at a rate of 1.22 mm/year.

In order to reconstruct the global circulation, and monitor its year to year variation, it is proposed to combine the baroclinic component deduced from the T-S profiles of the Argo floats with the barotropic component, deduced from their horizontal displacement. Satellite altimetry helps improving the barotropic component. The quality of the estimation relies on the robustness of the relation between barotropic and baroclinic components.

The last study aims at producing the best estimate of the ocean state combining Argo profiles, altimetry and an eddy permitting model over several years. A configuration involving 4D variational assimilation has been set up. This first year has been dedicated to the determination of the optimal parameters, mainly the length of the assimilation window, and to the evaluation of the impact of altimetry data, using synthetic and real data.

2 Quality control of large Argo datasets

Argo floats have significantly improved the observation of the global ocean interior, but as the size of the database increases, so does the need for efficient tools to perform a reliable quality control. We have developped a series of diagnostics based on the In Situ Analysis System (ISAS) run by Coriolis (one of the two Argo GDAC) to produce the real time weekly analysis of temperature and salinity (www.coriolis.eu.org).

ISAS uses estimation theory to combine information from previous knowledge on the ocean with all synoptic measurements, taking advantage of the relatively dense Argo coverage and of any other measurement. The method proposed here uses the analysis residuals to detect systematic errors. To be consistent with the hypothesis included in the method, the distribution of the residuals should not differ too much from a Gaussian, with zero mean and a standard deviation similar to the a priori error. Any bias or trend in the residual would indicate a sensor offset or drift. The analysis of their statistical and long term behavior thus provides a method to check the consistency of each data a) with the nearby measurements in time and space, b) with the climatology and c) with the a priori statistics expressed in the covariance scales and variance amplitude.

This method can be used in delayed mode and in real time to allow for early detection of errors. To discriminate between the error sources, it is better applied on the basic variables (temperature and salinity on depth levels), work on elaborate variables (isotherms or isopycnals reference, dynamical height) should be introduced at a later stage, as for example the Wong Method and the comparison with altimetry.

The tests were performed on the products made available by the Coriolis datacenter as NetCdf files containing the gridded temperature and salinity fields, the error maps, the data and the corresponding residuals. We have downloaded the global 2006 data set release, covering the 2000-2006 period. Since this data set is the result of a real time processing, it is absolutely necessary to perform some type of systematic control before any scientific interpretation. The Solo floats with pressure data problem for example are still part of this data set, since most of them had remained undetected until the beginning of 2007.

We operated as follows: 36 floats, all launched in the Atlantic, were selected. They represent the main instrument types (8 Solo, 15 Apex, 13 Provor) and include well behaved instruments and floats showing problems on salinity sensor or pressure data. The time series of data and residuals of these 36 floats were carefully screened and we illustrate here on a few examples the typical features of the two types of failure.

2.1 Salinity offset and drift detection

Float 6900272 was launched North-East of the Azores (Figure 1). The Temperature/Salinity diagram (Figure 2) shows a drift toward higher salinity values. A similar diagram constructed with the salinity residuals in layers deeper than 1000 m clearly shows that the center of gravity moves away from the origin along the salinity axis. This float had been flagged as bad shortly after days 1800 (refered to 01/01/2000). We see here that the sensor drift had started earlier.

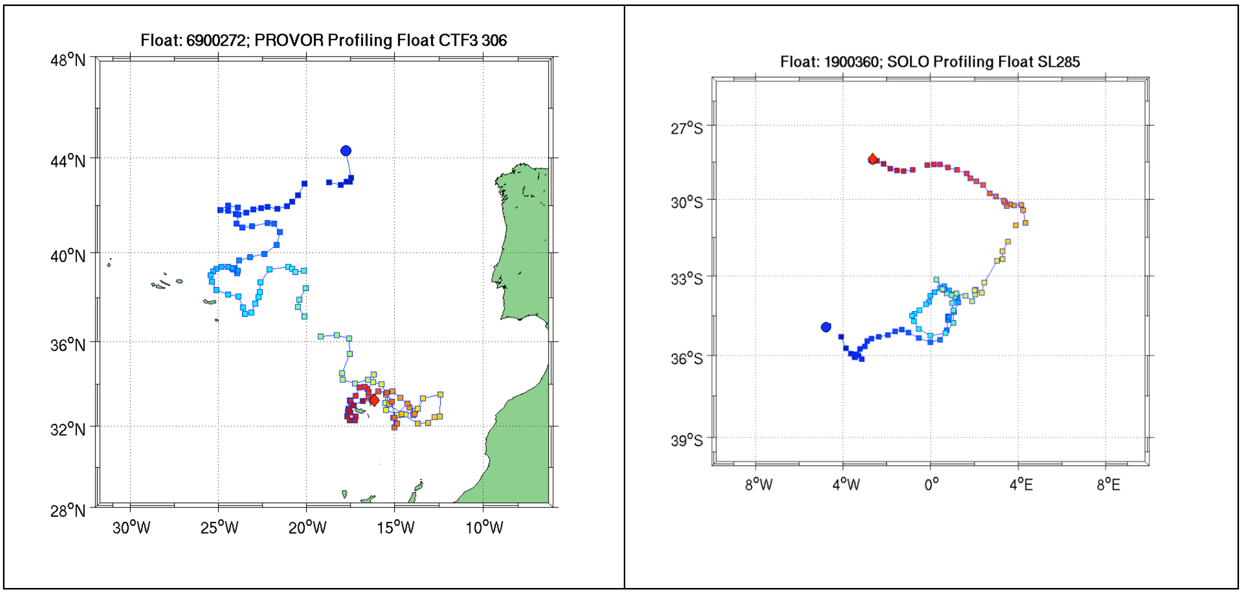

Figure 1 : Trajectories of the two floats selected to illustrate a salinity drift (left) and a pressure error (right).

The time series of salinity residuals averaged over a layer excluding the highly variable upper 400m has a clear trend not seen in temperature. In order to detect automatically this type of drift, a non parametric evaluation of the trend known as ***reverse arrangement test*** (Bendat and Piersol, 2000) has been used. The number of arrangement ***A*** of the salinity residuals is computed and a float will be considered as having a drift when the number of arrangements of the series falls out of the interval defined by +/- 2.7 standard deviation of a random distribution. When applied to the 36 selected floats, this test detected 6 floats as having a salinity drift (1 Solo, 3 Apex, 2 Provor), among which was float 6900272 . An additional test was performed on salinity to detect a salinity offset: The sensor is assumed to have an offset if the absolute value of the time mean of the salinity residuals is larger than 0.02. One Provor float was found to have an offset, that was confirmed by a later detailed analysis.

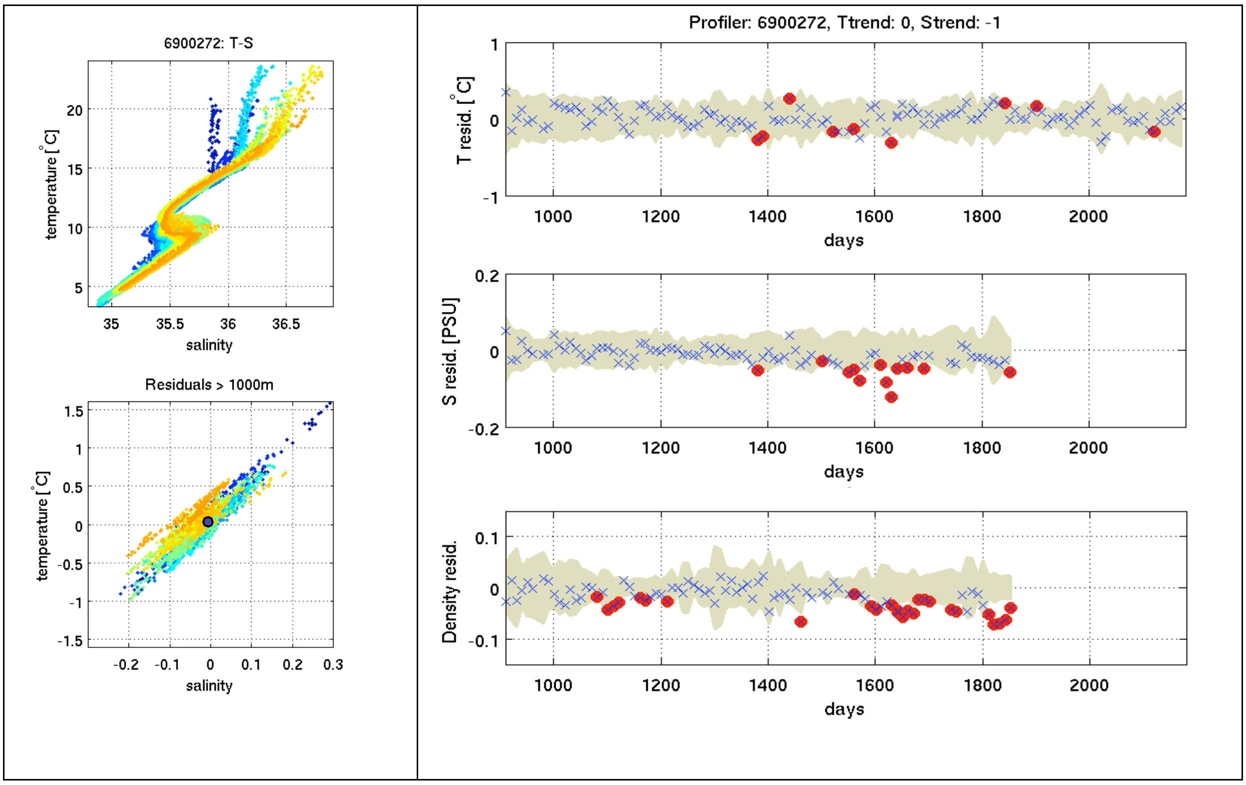

Figure 2 : T-S diagrams of a float with a salinity drift (left). Shown for the float measurements (top left) and for the deep residuals (bottom left). Time series of residuals (right). Top : temperature, middle : salinity, bottom : density. The result of the reverse arrangement test fot temperature and salinity is indicated above the top panel.

2.2 Error on pressure

An error in the pressure sensor leads to errors on temperature and salinity proportional to the vertical gradients of these properties. Since the temperature gradient is usually stronger, we focus on this variable to detect errors in the pressure data. The measurements given by the Solo float 1900360, launched in the south Atlantic in march 2004 and still transmitting data at the end of 2006, are shown here to illustrate the method. The profiles of innovation and residual show anomalous variations over time (see Figure 3): Deeper than 400 m, the level that corresponds to a change in the vertical sampling of the float, the sign of the residuals tend to alternate, with shallower profiles corresponding to strong negative anomalies. This behavior is related to the software error mentioned by the Argo centers.

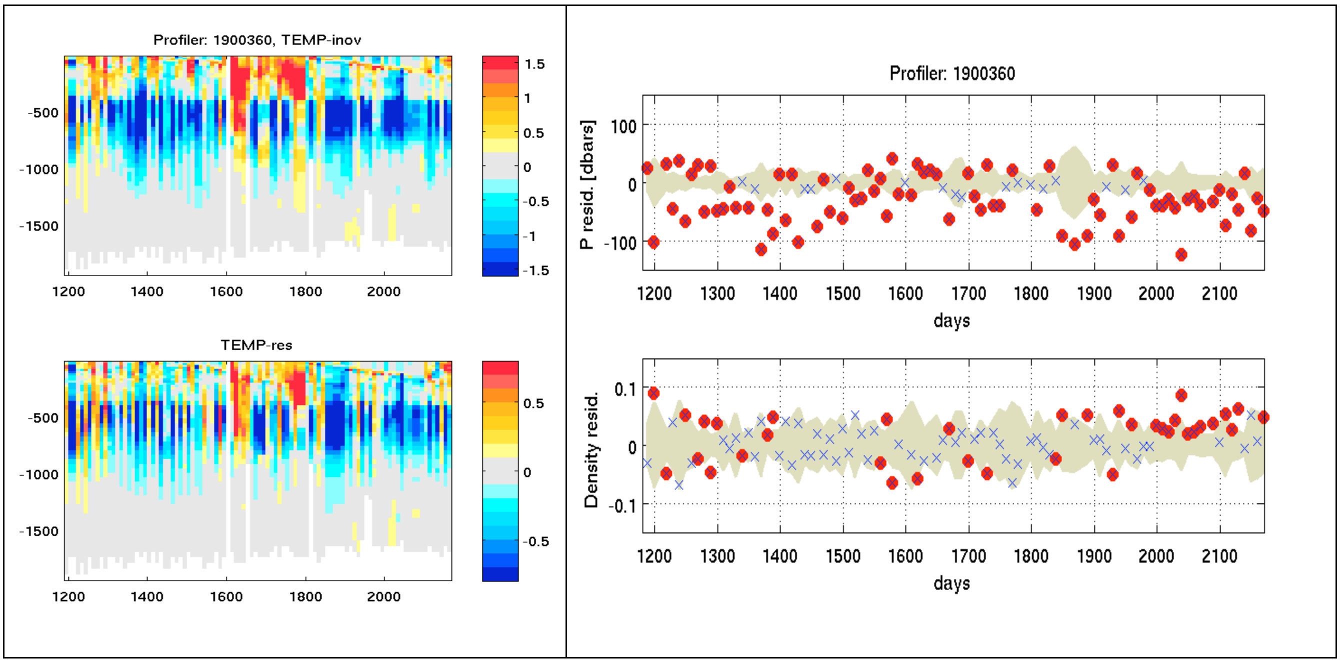

Figure 3 : Anomaly relative to the climatology for the temperature given by Solo float 1900360 (top left) and corresponding residual (bottom left) as a function of time and depth. Equivalent pressure residual deduced from the temperature residual (top right) and corresponding density residual.

In order to define a quantitative measure to detect this type of error we computed the pressure error ***dP*** equivalent to the temperature residual ***dT*** using the relation:

dT = (d***T***/d***P***) ***dP***

For each profile, this error is averaged over all levels deeper than 400m and the mean value of ***dP*** is compared to the corresponding vertical standard deviation. In the case of float 1900360, most of the mean pressure error are larger than the standard deviation, and the larger errors tend to be negative (Figure 3). In general, a negative pressure error leads to a positive density residual, but the natural variability of density may hide the systematic error. The pressure test is based on this pressure error series. The pressure sensor is assumed to have an offset over a given depth range when more than 70% of the mean pressure errors ***dP*** are larger than the vertical standard deviation and the RMS value of ***dP*** over time is larger than 20 dbars. This test successfully detected the 4 Solo floats which had been identified as problematic by the detailed analysis.

⇒ *More details on this work can be found in Gaillard et al., 2008*

3 Global ocean properties : interannual variability

Monthly global temperature and salinity fields from 0 to 2000m depth based on Argo measurements are used to analyze large-scale variability patterns on annual to interannual time scales during the years 2003-2007. Previous estimates of global hydrographic fluctuations have been derived using different data sets, partly based on scarce sampling. The substantial advantage of this study includes a detailed summary of global variability patterns based on a single and more uniform data base.

The basic materials for this study are the monthly gridded fields of temperature and salinity properties of the upper 2000m over the period 2003-2007 produced within the ARIVO project. These fields were obtained by optimal analysis of the large in-situ data set provided by the Argo array of profiling floats (http$://$www.argo.net). Complementary measurements from drifting buoys, CTDs and moorings are also used. Two important data sets have been excluded from the analysis because of proven or suspected biases. They are, first the XBTs and XCTDs for which uncertainties in the accuracy of the fall rate remain, and second, a small subset of Argo float profiles of type SOLO that suffer a labelling error in the pressure. The data set was downloaded from Coriolis data center (one of Argo Global Data Acquisition Center, or GDAC) at two dates: the period 2003-2006 was extracted in August 2007 and the year 2007 in January 2008. In total, the Argo measurements account for more than 95% of the data set.

The configuration is defined by the grid and the set of a priori information such as the reference climatology, a priori variances and covariances which are necessary to compute the covariance matrices. The analyzed field is defined on a horizontal ½° Mercator isotropic grid and is limited from 77°S to 77°N. There are 152 vertical levels defined between the surface and 2000m depth. The vertical spacing is 5m from the surface down to 100m depth, 10m from 100m to 800m and 20m from 800m down to 2000m depth. The reference field is the monthly World Ocean Atlas 2005.

3.1 Mean field and annual cycle for 2003-2007

An estimate of the large-scale variability patterns is derived from the hydrographic field during the time period 2003-2007 - a time period which is centered in the first decade of the 21th century. The mean 2003-2007 anomaly field and the first harmonic representing the annual cycle are computed and compared to their climatological counterparts. The quality of the estimation depends on data coverage information, which is quantified by the estimation error, it depends also on the interannual variability within the 5-year period. To analyze those changes in the near surface layer our results will be compared to estimates deduced from satellite derived SST measurements (NSST). Two time periods are used from the NSST field, a short term field during the same period 2003-2007 ($NSST_s$) and a long term estimation during the years 1990-2007 ($NSST_l$).

3.1.1 The mean 2003-2007 anomaly

Maximum differences between the mean temperature field and the corresponding WOA05 values lie between -0.7°C and 1.1°C and salinity differences range between -0.36pss and 0.38pss. However, a clear hemispheric asymmetry of the difference field can be observed as amplitudes of the zonal averages are considerably higher in the northern hemisphere (Figure

4). The difference field based on satellite derived SSTs ($NSST_s$-$NSST_l$) reveals a similar result (Figure 4a, red line). Maximum amplitudes are centered at about 60°N in both difference estimations and decrease to small values south of 30°N.

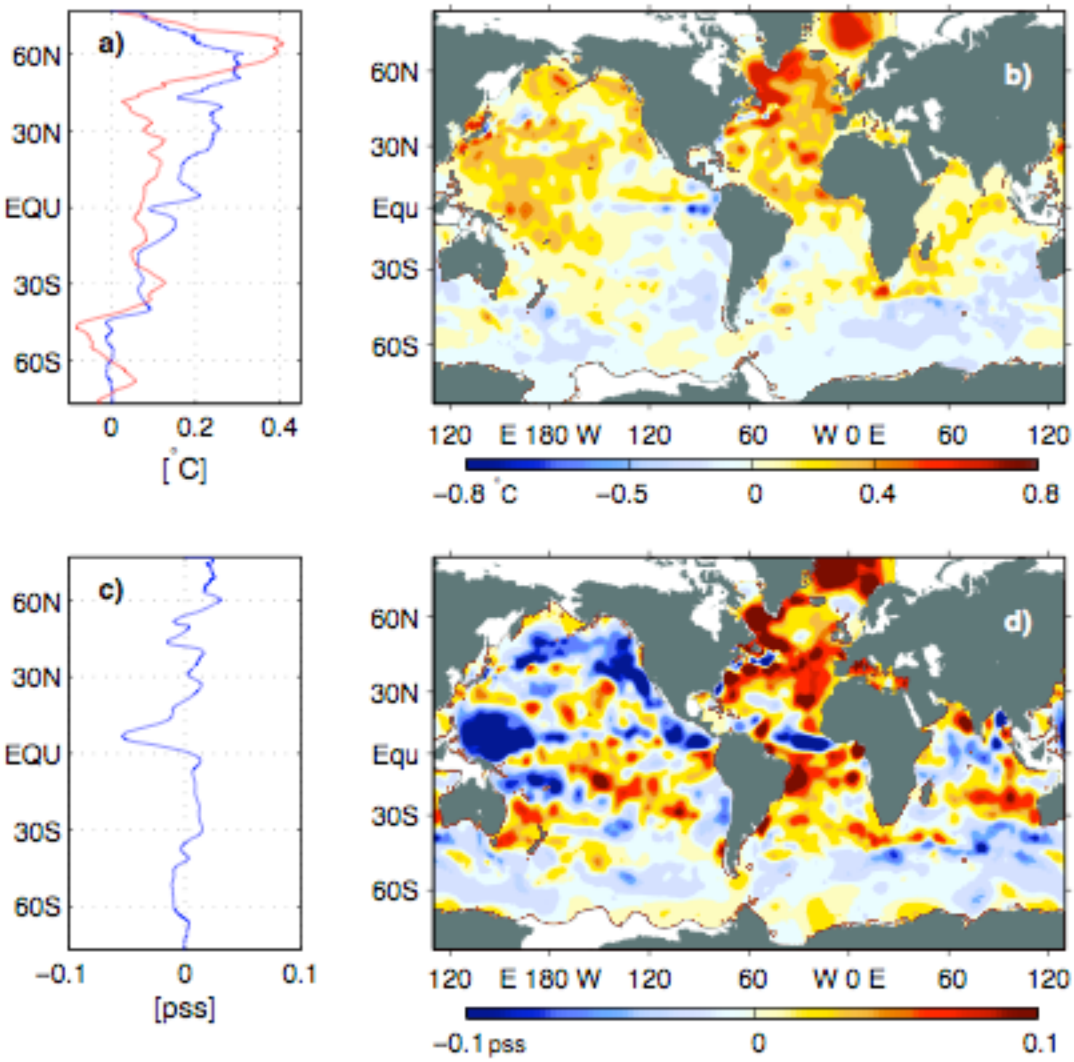

Figure 4 : Difference of the global zonal integrals of the dominant harmonic amplitude between WOA05 and ARIVO (2003-2007) temperature (a) and salinity (c) at 10m depth (blue) as a function of latitude. In addition, for the temperature field (a), differences between NOAA optimum Interpolation SST short-term (NSST, 2003-2007) and long-term (NSST_L, 1990-2007, red) are plotted. Horizontal maps show the amplitude of the dominant harmonic of temperature (b) and salinity (d) at 10m depth during 2003-2007. White masks in b) and d) refer to areas where the percentage of a priori variance is 99% or higher.}

The strongest temperature differences appear in the North Atlantic, subtropical West Pacific and in the North Pacific (Figure 4b). In these areas, values of ARIVO are generally higher indicating a warming signature which is dominant in the North Atlantic. Other areas of large-scale surface warming include the northern and entire western Indian Ocean basin and large parts of the southern subtropical Pacific and Atlantic. Warming of the Southern Ocean occurs only in the eastern Pacific. Differences in the rest of the Southern Ocean are slightly negative in the surface layer. Beside the Southern Ocean, surface cooling signatures are low and mostly restricted to the equatorial Pacific and the eastern subtropics of the Pacific and Indian Ocean. The global warming tendency also occurs at depth and the dominant surface warming in the northern hemisphere reaches down to more than 1000m.

Differences of SSS are restricted to the northern tropics, predominantly associated with a freshening pattern in the Pacific Warm Pool and in the domain of strong atmospheric variability due to the meridional movement of the tropical convergence zones (Figure 4d). Apart from that, zonal mean differences in the near surface layer between ARIVO and WOA05 remain low due to the fact that the difference estimation is characterized by a east-west distribution rather than meridional changes as it is the case for the temperature difference field (Figure 4b). Other regions of large-scale surface freshening can be observed in the northern and eastern Pacific, tropical Indian Ocean and large parts of the Bay of Bengal as well as the entire Southern Ocean between 40-60°S.

3.1.2 The annual cycle

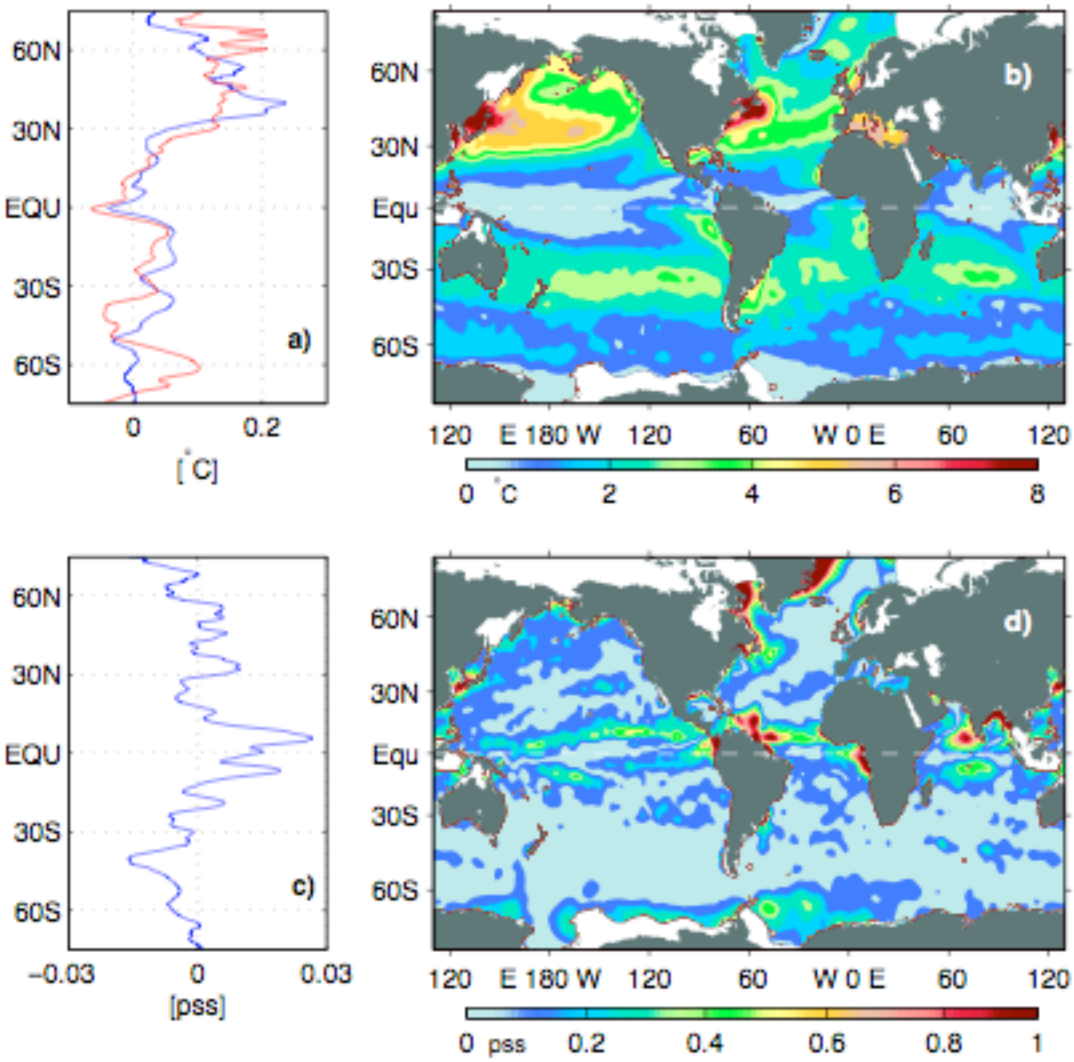

Figure 5 : Difference of the global zonal integrals of the dominant harmonic amplitude between WOA05 and ARIVO (2003-2007) temperature (a) and salinity (c) at 10m depth (blue) as a function of latitude. In addition, for the temperature field (a), differences between NOAA optimum Interpolation SST short-term (NSST, 2003-2007) and long-term (NSST$_L$, 1990-2007, red) are plotted. Horizontal maps show the amplitude of the dominant harmonic of temperature (b) and salinity (d) at 10m depth during 2003-2007. White masks in b) and d) refer to areas where the percentage of a priori variance is 99% or higher.}

Seasonal changes of SST range from 0.5°C up to 6°C (Figure 5 a and b). Amplitudes of the annual harmonic of SST become maximum at mid-latitudes and are characterized by a hemispheric asymmetry peaking in September in the northern. In the southern hemisphere the annual amplitude becomes maximum between 30-50°S in March. Comparisons using satellite derived SST measurements (NOAA Optimum Interpolation SST (NSST) have shown that the imbalance of the seasonal amplitude between the hemispheres also occurs in the high resolution measurements which indicates that the low amplitudes in the southern oceans do not result only from the lower data coverage in that region. The hemispheric asymmetry reflects the contrast between the two hemispheres in the distribution of land mass

In the upper 400m depth, the amplitudes of the annual harmonic of temperature decrease with increasing depth at mid-latitudes on both sides of the equator and the amplitudes reduce to values below 1°C at depth greater than 100m. The explained variance of the annual harmonic exceeds 80%$ of total variance in these areas.

3.2 Global averages time series

Global averages of heat content, freshwater content and steric sea level are evaluated from the ARIVO field during 2003-2007. To extract the interannual changes the annual harmonic is subtracted from each mean parameter.

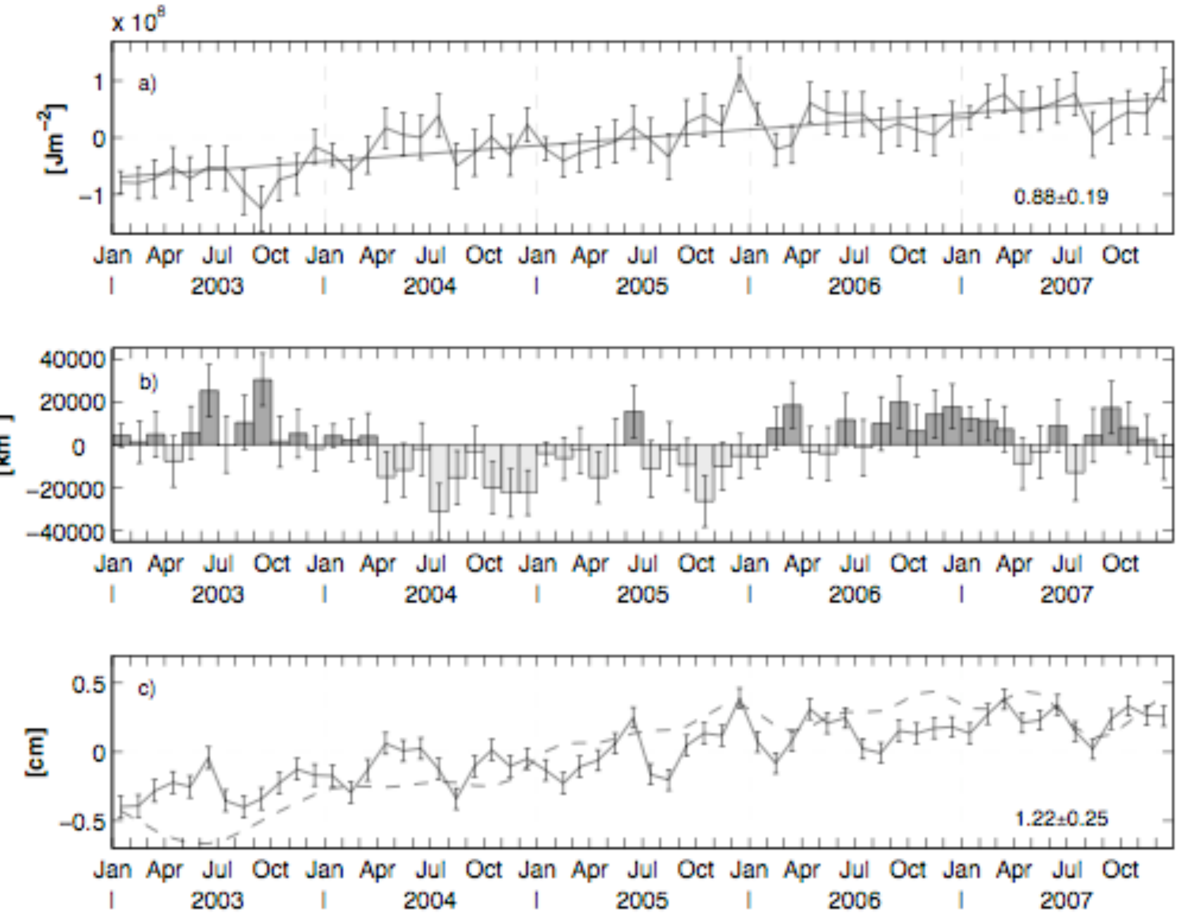

Figure 6 : Time series of global mean a) heat content b) freshwater volume variability and c) steric height. The parameters are evaluated from the monthly hydrographic field from 0-2000m depth. The global mean sea level as measured by satellite altimetry is added in c.

Figure 6a shows the variability of globally averaged deep ocean heat content computed from the monthly temperature anomaly fields. A considerable warming is visible from the year 2003 to 2007. The 5-year heat increase implied an average warming rate of 0.88pm0.19Wm^{-2}. Much of this increase in heat content comes from the Atlantic. Using satellite altimeter height combined with in situ temperature profiles the analysis of Willis (2004) revealed an oceanic warming rate of 0.86pm$0.12 Wm^{-2}. Their warming rate estimation is of similar size as our estimation indicating that either the layer 750-2000m depth only little contributes to the average warming or the differences are associated to interannual fluctuations during the different time period used for both estimations. Levitus (2005) have shown that the world ocean heat content (0-3000m) increased at a rate of 0.2 Wm^{-2}. This value is much lower since it is an estimation over a longer and earlier time period.

With the ARIVO product a global average of the freshwater change in the upper 2000m depth can be established for the first years of Argo. Freshwater corresponds to changes in mean salinity that can be due to E-P, river runoff and ice melting. Mass changes due to the import of freshwater from continents are not debated and need to be discussed in future studies. The global average of freshwater content anomalies is dominated by interannual changes. The 5-year trend from 2003 to 2007 is very small (Figure 6b). During 2003, positive freshwater content can be observed which changes sign in 2004 to 2005. In the years 2006 and 2007, an increase in freshwater content occurs.

Globally averaged steric sea level variability shows a positive trend and the rate of changes from the years 2003 to 2007 can be estimated as 1.22±0.25 mm/year (Figure 6c). Interannual fluctuations of global steric sea level exist but are small compared to the long term variability. In Figure 6c, the global mean sea level as measured by satellite altimeter is added for the same time domain (dashed line). On this short time scales based in this analysis, total sea level includes changes due to temperature and salinity related steric expansion as well as mass changes. The sea level rise based on satellite measurements accounts 2.09 mm/year during 2003-2007. Thus, the 5 year changes based on steric contribution alone constitutes about 60% to the total sea level rise during that time. The two time series are in good agreement, especially during the second half of the measurement period when the data coverage has been increased. In the years 2003 and 2004, deviations between the two independent data sets are stronger compared to the second half and the steric sea level component appears to be smoothed compared to the satellite derived information as large spatial variabilities are not sufficiently resolved by the ARIVO product. This suggests that the increase of data coverage during 2006 contributes to the better agreement.

⇒ *More details on this work can be found in von Schuckmann et al., 2008*

4 Variations of the large scales oceanic circulation

4.1 Diagnostic Methods

The objective of this work is to reconstruct the oceanic circulation field and its variations from a simple diagnostic method: T, S profiles give the baroclinic circulation through the thermal wind relation and a reference velocity field is used to deduce the barotropic circulation

A preliminary study has shown that ARIVO T, S fields allow to reconstruct a mean baroclinic circulation in the North Atlantic that is comparable to those obtained from ECCO or Drakkar (ORCA 0.25) model outputs. The spatial structures of observed and modeled baroclinic circulation interannual variability are also similar (first EOF mode) although the amplitude of the variability obtained from T, S observations is larger (Figure 7).

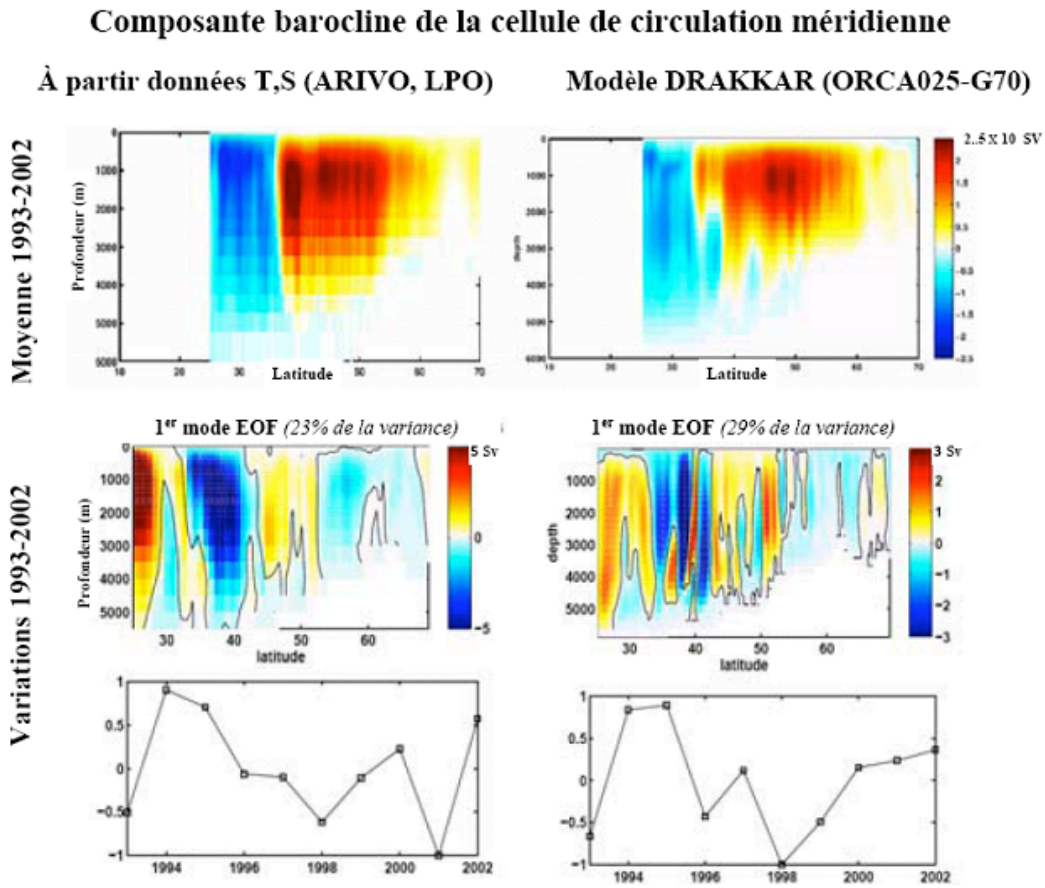

Figure 7 : Baroclinic component of the meridional circulation Mean over 1993-2002 from (A) T, S data (ARIVO, LPO) and (B) Drakkar (ORCA025-G70) model. Interannual variations from 1993 to 2002: first EOF mode obtained from (C) T, S data (ARIVO, LPO) and (D) Drakkar (ORCA025-G70) model

The main part of the work done in 2008 was to use the Argo float displacements at 1000m depth to deduce a mid-depth reference velocity field. The complementarities of the trajectory data with altimetry data were investigated. Indeed, strong correlations exist between mid-depth velocity anomalies deduced from Argo float displacements and surface geostrophic velocity anomalies from altimetry at middle and high latitudes (see Figure 9).

After computing mid-depth velocity anomalies from Argo float displacements, we investigated the nature of the correlation with geostrophic velocity anomalies at the surface. We then assessed how the two vertical modes (barotropic and first baroclinic) would partition to best explain the collocated observed anomalies of the surface (derived from satellite altimetry) and intermediate-depth (derived from trajectories of floats) velocities.

4.2 Mean Flow and variability from Argo floats

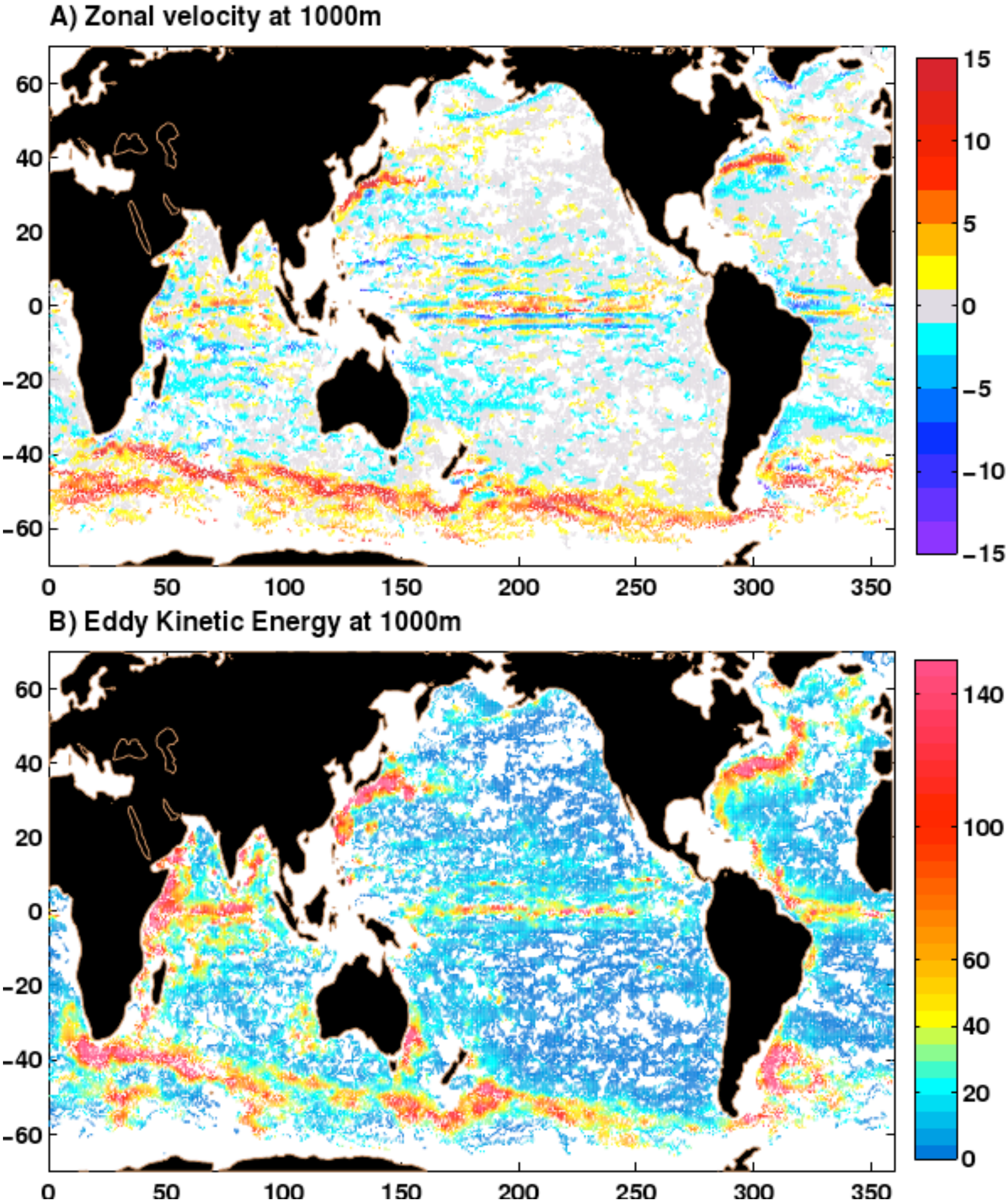

Figure 8 : Mean zonal velocities (in cm s^{-1}) at 1000 m depth deduced from the Argo float displacements. Zonal velocities are positive eastward. b) EKE (in cm^2 s^{-2}) at 1000 m depth

Argo-derived mid-depth velocities from August 1997 to May 2007 were obtained from the Yomaha'07 dataset [Lebedev et al., 2007]. Our purpose is to compare surface and mid-depth velocity anomalies. A mid-depth mean for each component u and v was first computed by averaging all data within 500 km of the position of a velocity estimate, applying an elliptical Gaussian weight w function of the distance. On Figure 8a, alternating zonal jets in the equatorial Atlantic (already observed with Argo and Marvor floats by Ollitrault et al. [2006]) and in the equatorial Pacific (also observed with Lowered Acoustic Doppler Current Profiler measurements by Gouriou et al. [2006]) are particularly noticeable. Large EKE values at 1000 m depth are associated with major oceanic currents (Figure 8b).

4.3 Correlation between Surface and Mid-depth Velocity Anomalies

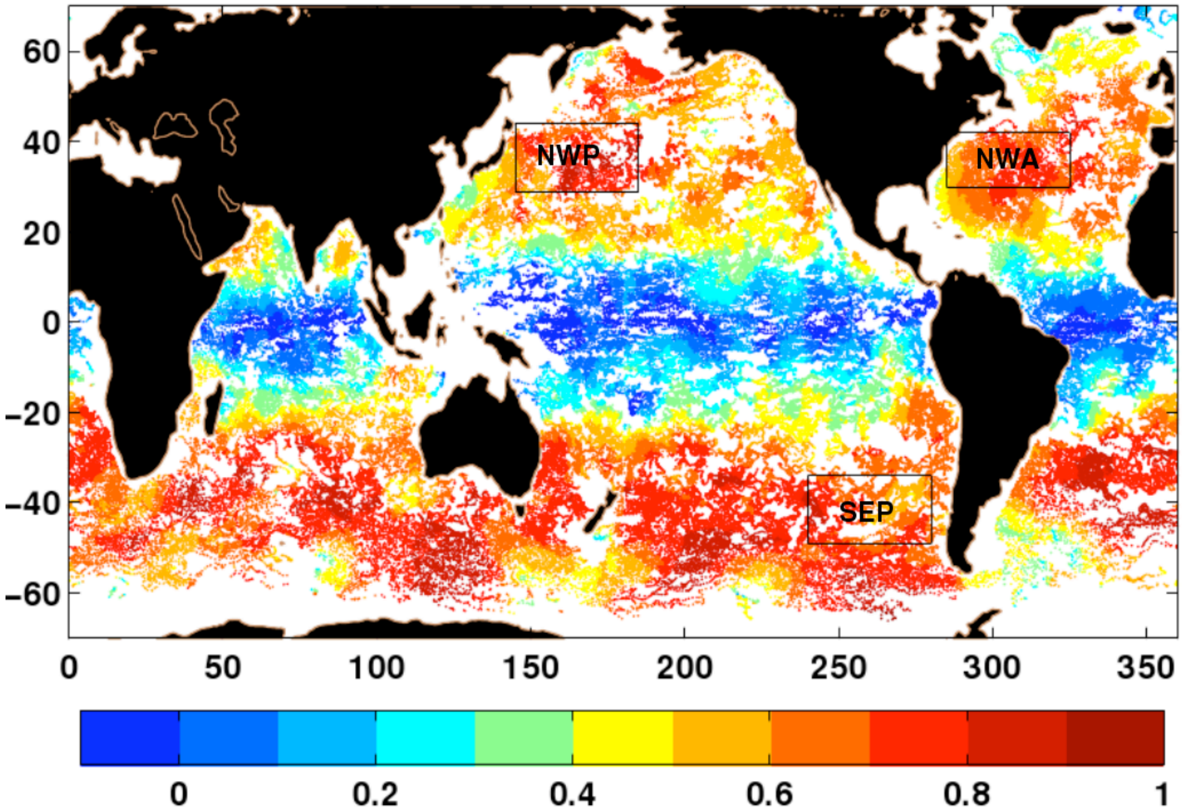

Figure 9 : Correlation between Argo float zonal velocity anomalies (relative to the mean velocity shown in Fig. 1 at 1000m depth and geostrophic zonal velocity anomalies at the surface deduced from altimetric sea level

Figure 9 shows correlations between the surface and the 1000 m depth meridional velocity anomalies (a similar map is obtained for the zonal component). A correlation coefficient is computed at each observation location from all the points at the same depth within a 500 km distance. The correlation map exhibits high values at middle and high latitudes, and low values at latitudes below 15-20°. Taking all the meridional (zonal) velocity observations poleward of 20°, the global correlation coefficient is 0.56 (0.54).

Further analyses in three specific regions (NWP, NWA and SEP, see Figure 9) were performed. They shown that in region of high EKE (e.g NWA or NWP) the correlation is due to large eddies with wavelength 300-400 km. In areas of lower eddy kinetic energy such as SEP, the correlation is largely due to structures less than 300km wavelength and period longer than 8 months.

4.4 *Partition between the Barotropic and the First Baroclinic Modes*

We then assessed how the two vertical modes (barotropic and first baroclinic) would partition to best explain the collocated observed anomalies of the surface (derived from satellite altimetry) and intermediate-depth (derived from trajectories of floats) velocities.

To quantify the variation of the velocity amplitude with depth, we compute the linear regression coefficient between the surface and the mid-depth velocity anomalies (Figure 10a). This regression coefficient (R_v^{1000}) is always positive and ranges from 0.05 to 0.6, reflecting the baroclinicity of the flow. For a purely barotropic anomalous flow, this regression coefficient would be one; in case of an anomalous flow projecting entirely onto the first baroclinic mode, this ratio would simply be equal to F1 (1000)/F1 (0) where F1 (z) is the vertical structure of the first vertical baroclinic mode [Chelton et al., 1998].

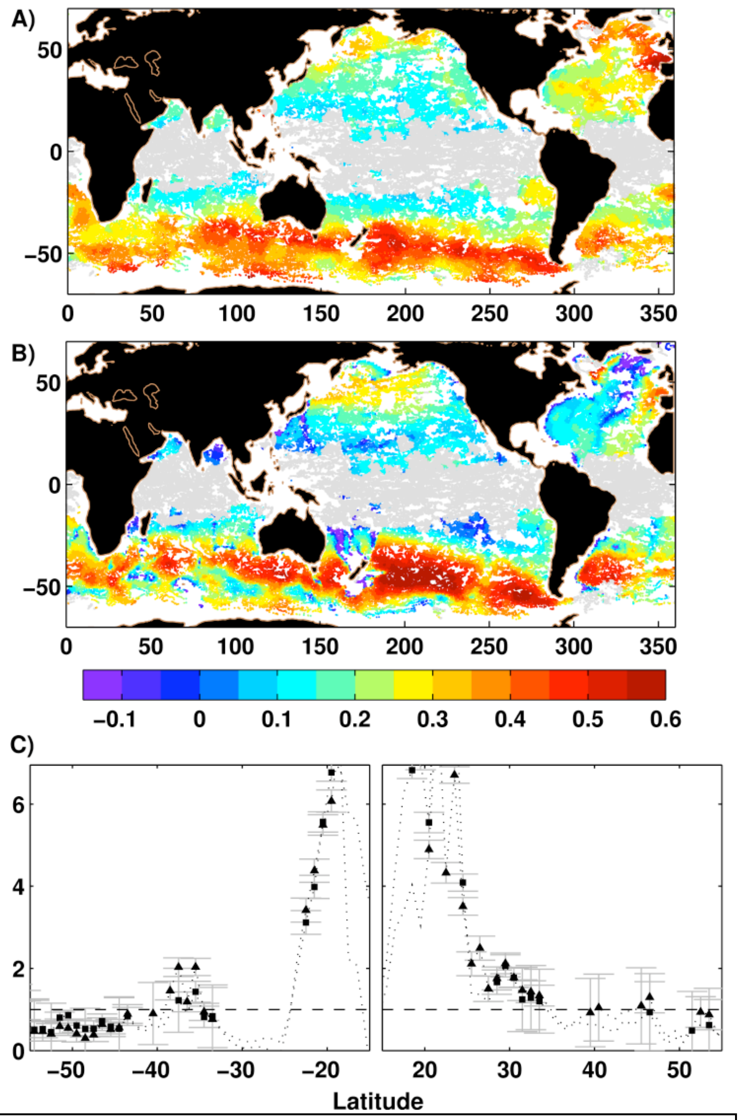

Figure 10 : Linear regression coefficients Rv1000 between meridional velocity anomalies at 1000 m depth and those at the surface. Grey color is used when the correlation (Fig 2) is less than 0.35. b) F1 (1000)/F1 (0), ratio of the first baroclinic vertical mode at z = 1000 m to the surface value. c) Estimated ratio B/A of the first baroclinic mode to the barotropic mode contributions for surface velocity anomalies as a function of latitude. Triangles highlights values of the B/A ratio when the correlation between Rvz and F1 (z)/F1 (0) is greater than 0.4 at a given latitude. Squares are similar but for Ru. Bars represent a 95% confidence interval for the fit.

There is an apparent linear relation between F1 (1000)/F1 (0) and R_v^{1000} with a global correlation of 0.6. The correlation is much weaker (< 0.3) in the North Atlantic however (Figure 10a and Figure 10b)

If the anomalous flow is the sum of a barotropic and a first baroclinic mode one can expect a linear relation between R_v^{1000} and F1 (1000)/F1 (0)

We checked if such a relation exists at a given latitude y:

$$R^z = \mathcal{A}(y) + \mathcal{B}(y) \times \frac{F_1(z)}{F_1(0)} + \varepsilon$$

The ratio B/A obtained for each 1◦ latitude band, shows a clear dependence on latitude (Figure 10c).Its structure is more or less symmetric with respect to the Equator, with maximum values up to 3-7 occurring around 20◦ S and

20◦ N, whereas values close to 1 or lower occur poleward of 40◦ S and 35◦ N. The smallest values, close to 0.5, are reached in the Antarctic Circumpolar Current (ACC) region.

4.5 Conclusion

- Nature of the correlation between geostrophic surface velocity anomalies derived from altimetry and the mid-depth velocity anomalies derived form Argo float displacements: The correlation of surface anomalies with depth can be dependent on the wavenumber and period. In region of high EKE, there are evidences that the correlation is due to large eddies with wavelength 300-400 km, in accordance with a vertically coherent velocity structure observed for such anomalies [Swart et al., 2008]. In areas of lower eddy kinetic energy such as SEP, the correlation is largely due to structures less than 300km wavelength and period longer than 8 months.
- Fraction of u or v components in the first baroclinic mode versus the barotropic one, at the surface: The partition, valid for the part of the surface variability correlated with the one at mid-depth, is latitude dependent: the first baroclinic mode dominates equatorward 30° while the barotropic mode is more important poleward. This is consistent with the results of [Guinehut et al. 2006]. Finally, one can expect that the increase of Argo dataset and further corrections on mid-depth velocities estimates will improve the determination of the partition between the barotropic and the first baroclinic modes.

4.6 References

Gouriou, Y., and T. Delcroix, and G. Eldin (2006), Upper and intermediate circulation in the western equatorial Paci_c Ocean in October 1999 and April 2000, Geophys. Res. Lett., 33, L10603, doi:10.1029/2006GL025941.

Guinehut, S., P.-Y. Le Traon, and G. Larnicol (2006), What can we learn from global altimetry/hydrography comparisons?, Geophys. Res. Lett., 33, L10604, doi:10.1029/2005GL025551.

Lebedev, K. V., H. Yoshinari, N. Maximenko, and P. Hacker (2007), Yomaha'07: Velocity data assessed from trajectories of argo floats at parking level and at the sea surface, Tech. Rep. No. 4(2), IPRC Technical Note No. 4(2), June 12.

Ollitrault, M., M. Lankhorst, D. Fratantoni, and P. Richardson (2006), Zonal intermediate currents in the equatorial Atlantic Ocean, Geophys. Res. Lett., 33, L05605, doi: 10.1029/2005GL025368.

Swart, N. C., I. J. Ansorge, and J. R. E. Lutjeharms (2008), Detailed characterization of a cold Antarctic eddy, J. Geophys. Res., 113, C01009, doi:10.1029/2007JC004190

⇒ *More details on this work can be found in Cabanes et al., 2008*

5 4D-variational assimilation of Argo profiles and altimetry

The aim of the project is to increase our understanding of the oceanic variability through the use of analyses produced by a 4D-variational assimilation method. For this purpose, the method is applied to an eddy-permitting configuration of the North Atlantic using the primitive equation model OPA (version 8.2; Madec et al. 1998). The configuration of the prognostic model is the following:

- Domain : North Atlantic (latitude 20°S - 70°N, longitude 98°W –14°E).
- Resolution : horizontal 1/3° x 1/3°cos(latitude) (280 x 361 grid points), 43 vertical levels. Time step : 2880 s.
- Bilaplacian horizontal diffusion, vertical diffusion based on a TKE scheme.
- Bathymetry built from Smith et Sandwell. Key passages for overflows manually corrected.
- Daily forcing from NCEP reanalysis II.

The adjoint (Weaver et al. 2003) uses a constant vertical diffusivity that is updated from the forward run. Error covariance matrices are diagonal for observations and the background. The assimilation scheme uses the forward full non-linear model in order to lengthen the assimilation window. The 3D initial state (hydrology, velocity) are the only state variables that the method changes to get closer to the assimilated data. Since little is known about the potential of such a method when it is combined with a realistic GCM that uses an eddy-permitting horizontal resolution, twin experiments with synthetic data were conducted before using real observations.

5.1 Synthetic data: Determining the best window length

All three windows show a significant reduction of the error compared to the solution with no assimilation (see Figure 11 for temperature after 180 days). The error is measured by the typical distance (here using the rms) to the known true state. Maximum errors are found below the mixed layer and decrease with depth. After 180 days of assimilation, the worse window is the six-month-long one (W6). After almost a year of assimilation, the best window is the the three-month-long one (the six-month window profile W6 is not shown at 360 days since there is almost no improvement between days 180 and 360).

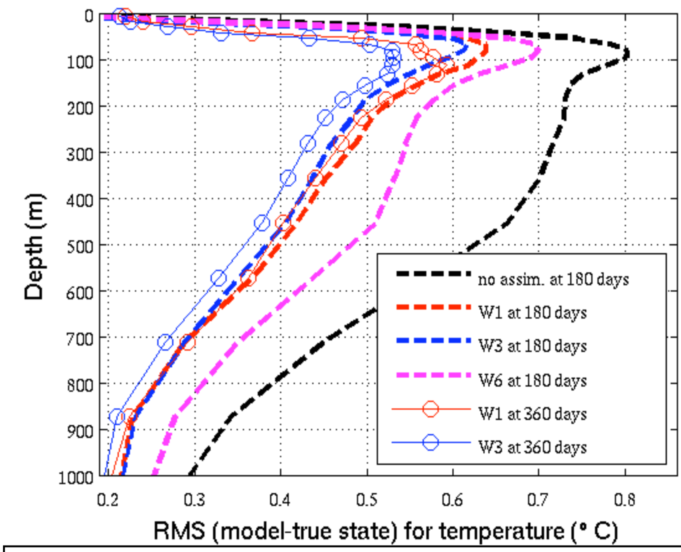

Figure 11 : rms of the temperature differences between the model state and the true state. The model state is either the state without assimilation (black) or the analysis with a window of 1, 3 or 6 months (resp. red, blue and magenta). The rms is calculated over the whole domain after 6 (dashed) and 12 months (circles) of assimilation.

5.2 Impact of the assimilation of sea surface height maps

Maps of absolute dynamic topography (homogeneous datasets based on two satellites) provided by AVISO every seven days are assimilated for years 2000-2002 using a 3 month-long window. Their model counterpart consist of seven-day-long averages of the model free surface height. The first guess of the assimilation on January 1, 2000 is the model state after a five-year-long spin-up forced with the daily NCEP II reanalyses. This spin-up starts at rest from Reynaud seasonal climatology (Reynaud et al., 1998).

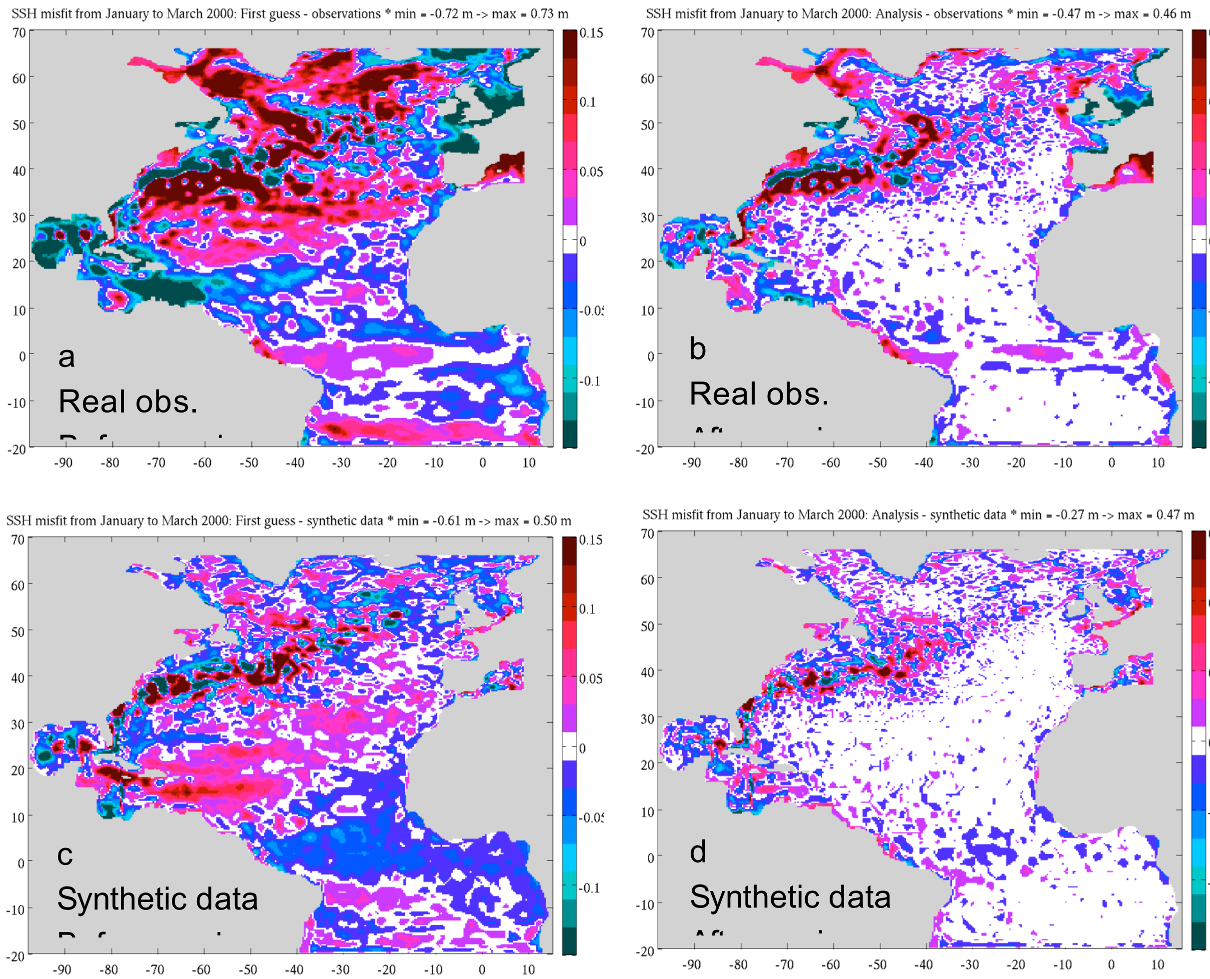

Figure 12 : Sea surface height misfit (SSH, meters) averaged on the first window (January to March 2000) between the model and the data. Left (right) panels: model without (after) assimilation. Upper panels: misfit to real SSH. Lower panels: misfit to synthetic SSH (twin experiments).

Before assimilation, SSH misfits (model-data) are larger for real observations than for synthetic data (Figure 12ac). However they have similar maximum amplitudes and similar patterns composed of large-scale and meso-scale structures. For both type of assimilated data, those misfits after assimilation (residuals) have been significantly reduced (Figure 12bd) even in region of strong meso-scale activity. The amplitude of the residuals are close to the error on the data, this error being larger where eddies are numerous due to an increased representativity error (eddies are not resolved in this configuration). The assimilation of real SSH behaves like the assimilation of synthetic SSH. We can then expect improved hydrology (as in Figure 11) and velocities (not shown) on the top thousand meters when real SSH is assimilated. This is confirmed by comparisons of the model hydrology to Argo profiles of temperature and salinity used as independent observations (not shown). From twin experiments, we also expect that the combined assimilation of SSH maps and Argo profiles will further improve the analyses (ongoing work).

6 Publications

Journals

Cabanes, **C**., **T. Huck**, A. Colin de Verdière, **M. Ollitrault**, Partition between barotropic and first baroclinic mode from Altimetric Velocities and Argo Float Mid-depth Displacements, submitted to GRL

Gaillard, F., E. Autret, V.Thierry, P. Galaup, C. Coatanoan, and T. Loubrieu , 2008 : Quality control of large Argo data sets. JOAT, In Press.

von Schuckmann, K., F. Gaillard and P.-Y. Le Traon : Global hydrographic variability patterns during 2003-2007. Submitted to JGR.

Scientific conferences

Cabanes, C., T. Huck, A. Colin de Verdière, M. Ollitrault, Partition between barotropic and first baroclinic mode from Altimetric Velocities and Argo Float Mid-depth Displacements, Euro-Argo Users Workshop, Southampton, June 2008.

Cabanes, C., T. Huck, A. Colin de Verdière, M. Ollitrault, Partition between barotropic and first baroclinic mode from Altimetric Velocities and Argo Float Mid-depth Displacements, GMMC 2008, Toulouse Oct 2008.

Ferron, B. : Assimilation 4D-variationnelle de la hauteur de surface de la mer dans un modèle Atlantique Nord "eddy permitting", Colloque National LEFE - Assimilation de données, Paris, 1-2 Déc. 2008 (Poster).

Gaillard, F., K. Von Schuckmann, L. Petit de la Villéon : Observation of near ocean surface variability: data synthesis and analysis. GOSUD/SAMOS meeting(oral presentation, Seattle, Juin 2008)

Gaillard, F, K. Von Schuckmann : ISAS-V4: le nouvel outil d'analyse des mesures in-situ. Application à l'étude de la variabilité interannuelle de l'océan global . Journée du Calcul scientifique. Brest, Mai 2008.

Gaillard, F., A. Melet : Interannual to decadal variability of the North Atlantic over the last 30 years. EGU Vienne (Avril 2008). Poster

Gaillard, F., E. Autret and V. Thierry. Quality control of large Argo datasets. EuroArgo User group meeting, Oral presentation, Southampton, june 2008.

Gaillard, F., E. Autret, R. Charraudeau, K. Von Schuckmann : In-situ data validation and global synthesis. MERSEA final conference, Paris (mai 2008), Oral presentation.

Thierry, V, E. de Boisséson, F. Gaillard, P. Lherminier, E. Louarn, H. Mercier, P. Morin. Combining Ovide and Argo data to monitor and understand water masses variability in the North –Atlantic. Mersea final meeting. Paris, Avril 2008. Poster

Thierry, V., F. Gaillard, P. Lherminier, H. Mercier: Impacts of global changes on the North-Atlantic water masses: Monitoring and understanding the variability. First Marine board forum. Ostende. May 2008. Poster.

Von Schuckmann, K., F. Gaillard and P-Y. Le Traon : Global hydrographic overview of ocean variability, EGU Vienne (Avril 2008). Poster

Von Schuckmann, K., F. Gaillard and P-Y. Le Traon : Global hydrographic variability patterns during 2003-2007. GMMC. Toulouse, Octobre 2008. Poster

Von Schuckmann, K., F. Gaillard, and P.-Y. Le Traon : Hydrographic variability patterns in the tropical oceans during 2003-2007. AGU, San Francisco, December 2008, Poster.

Von Schuckmann, K., F. Gaillard, and P.-Y. Le Traon : Global hydrographicvariability patterns during 2003-2007. Godae meeting. Nice, November 2008. Poster.

Workshops,

Réunion annuelle du WGOH du CIEM (Aberdeen , mars 2008)

Réunion SMOS-Tosca (Paris, 3-4 avril 2008)

Public outreach

Gaillard, F. : Variabilité de l'océan et changement climatique: Modifications observées à l'échelle du globe et en Atlantique Nord. Conférences du centre Ifremer de Brest, Avril 2008.

Gaillard, F.: Conférence de presse Campagne OceanoScientific de la Solocéane, Salon Nautique, Paris, 9 Décembre 2008.

Reports

Gaillard, F. and R. Charraudeau: ISAS-V4.1b: Description of the method and user manual. Rapport LPO 08-03

Gaillard, F. and R. Charraudeau: New climatology and statistics over the global ocean. MERSEA del. 5.4.7. June 2008.

Gaillard, F. :Synthesis of indicators over the gloal ocean: Data/model comparison. MERSEA del. 5.4.8. July 2008.